Correction

PHYSICS

Correction for "Probing large viscosities in glass-formers with nonequilibrium simulations," by Vikram Jadhao and Mark O. Robbins, which was first published July 10, 2017; 10.1073/pnas.1705978114 (*Proc Natl Acad Sci USA* 114:7952–7957).

The authors note, "It has been brought to our attention that representing the experimentally measured Newtonian viscosity value by a set of points on a horizontal line in Fig 2*B* might mislead readers into thinking that measurements were made at the indicated strain rates. Low–strain-rate data points in Fig. 2*B* at pressures of 0.1, 100, 200, 300, 400, and 500 MPa are attributed to references 20, 24, and 25 when the points do not correspond to actual experimental data. The *y*-axis values for these points are the experimental low-shear viscosities for the corresponding pressures reported in ref. 20. We have revised Fig. 2*B* to remove these 24 data points (4 per curve) along the 0.1, 100, 200, 300, 400, and 500 MPa lines. The revised figure depicts the same experimental Newtonian viscosity value for each pressure by a horizontal line to indicate the limiting low–strain-rate behavior. We hope that this change eliminates any unintended confusion. This revision does not affect any of the conclusions drawn in the original article." The corrected Fig. 2 and its corrected legend appear below.

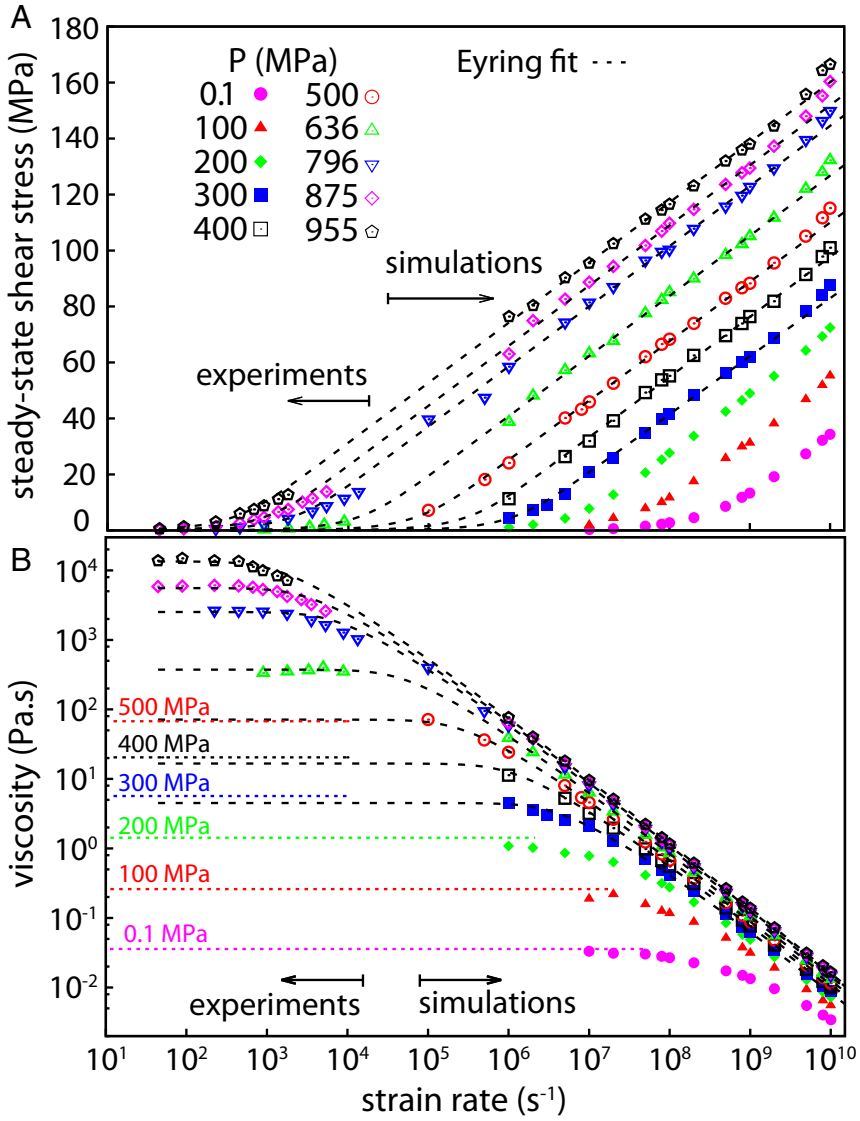

Fig. 2. Steady-state shear stress σ and viscosity η of squalane as a function of strain rate $\dot{\gamma}$. Stress σ vs. $\dot{\gamma}$ at T = 293 K for P from 0.1–955 MPa (*A*) and viscosity $\sigma/\dot{\gamma}$ vs. $\dot{\gamma}$ (*B*) for the same systems. Symbols for $\dot{\gamma} \geq 10^5 s^{-1}$ correspond to MD simulation results. Data points at lower rates for $P \geq 636$ MPa are from nonequilibrium experiments (24, 25). For $P \leq 500$ MPa, only low-rate measurements have been reported (20). The limiting Newtonian viscosities (20) are indicated by horizontal dotted lines that are labeled above by the pressure. These dotted lines are extended to rates where they can be directly compared with simulation results or to the Newtonian limit of Eyring fits (black dashed lines) to simulation data for $10^6 s^{-1} \leq \dot{\gamma} \leq 10^9 s^{-1}$. These fits for $P \geq 300$ MPa (*A*) show a linear dependence of stress on $\log\dot{\gamma}$ for high $\dot{\gamma}$ and (*B*) extrapolate to the Newtonian viscosity at low rates. For $P \leq 500$ MPa, simulations reach the Newtonian limit without extrapolation.

www.pnas.org/cgi/doi/10.1073/pnas.1715376114

Probing large viscosities in glass-formers with nonequilibrium simulations

Vikram Jadhao[a,b] and Mark O. Robbins[b,1]

[a]Department of Intelligent Systems Engineering, Indiana University, Bloomington, IN 47408; and [b]Department of Physics and Astronomy, Johns Hopkins University, Baltimore, MD 21218

Edited by Pablo G. Debenedetti, Princeton University, Princeton, NJ, and approved June 1, 2017 (received for review April 10, 2017)

For decades, scientists have debated whether supercooled liquids stop flowing below a glass transition temperature T_{g0} or whether motion continues to slow gradually down to zero temperature. Answering this question is challenging because human time scales set a limit on the largest measurable viscosity, and available data are equally well fit to models with opposite conclusions. Here, we use short simulations to determine the nonequilibrium shear response of a typical glass-former, squalane. Fits of the data to an Eyring model allow us to extrapolate predictions for the equilibrium Newtonian viscosity η_N over a range of pressures and temperatures that change η_N by 25 orders of magnitude. The results agree with the unusually large set of equilibrium and nonequilibrium experiments on squalane and extend them to higher η_N. Studies at different pressures and temperatures are inconsistent with a diverging viscosity at finite temperature. At all pressures, the predicted viscosity becomes Arrhenius with a single temperature-independent activation barrier at low temperatures and high viscosities ($\eta_N > 10^3$ Pa·s). Possible experimental tests of our results are outlined.

glass transition | nonequilibrium systems | molecular dynamics simulations | rheology | supercooled liquids

Glass-forming liquids flow rapidly when hot but appear to become quenched into a fixed disordered structure at low temperatures. Researchers continue to debate whether this represents a transition to a new phase of matter or merely a slowing of dynamics beyond the observable range of time scales (1–12). Experimentalists typically measure the rise in the Newtonian viscosity η_N as a liquid is cooled and define the glass temperature T_g as the value where η_N reaches 10^{12} Pa-s. This temperature identifies when the dynamics become difficult to measure, rather than a fundamental transition where η_N diverges and the material enters a new state.

Perhaps the simplest model of glassy dynamics is that motion is always thermally activated. If viscous flow requires activation over a free energy barrier of height ΔH, then the viscosity will scale inversely with the activation rate:

$$\eta_N = \eta_0 \exp[\Delta H/k_B T], \quad [1]$$

where k_B is Boltzmann's constant and η_0 is a characteristic high-temperature viscosity. When ΔH is independent of temperature, plots of $\log \eta_N$ against $1/T$ form straight lines. Supercooled liquids that follow this Arrhenius behavior are called strong glass-formers (1). Fragile glass-formers show a more rapid, super-Arrhenius rise, indicating that ΔH grows with decreasing T (1). Ambient pressure data for the simple hydrocarbon molecule squalane in Fig. 1 are typical of fragile glass-formers. The slope of this curve rises by more than a factor of 3 over the experimentally accessible range from 10^{-3} to 10^8 Pa·s, indicating a proportionate increase in the activation barrier.

A central question is whether ΔH continues to rise slowly with decreasing temperature or diverges at a finite temperature T_{g0} (4, 13–15). Data for fragile glass-formers is often fitted to the Vogel–Fulcher–Tammann (VFT) model (16–18),

$$\eta_N^{\mathrm{VFT}} = \eta_0 \exp\left[\Delta H_0/k_B\left(T - T_{g0}\right)\right], \quad [2]$$

where $\Delta H = \Delta H_0/(1 - T_{g0}/T)$ diverges at T_{g0} and the constant ΔH_0 is the activation barrier at high temperatures. Fig. 1 shows published VFT fits to two sets of squalane data (19, 20) that illustrate a common problem. Excellent fits can be obtained to experiment, but extending data to lower temperatures frequently leads to a significant decrease in T_{g0}. Hecksher et al. have recently considered data for a wide range of molecular glass-formers and shown that they are all equally well fitted by theories where η_N diverges at a finite T_{g0} or only at zero temperature (21). They concluded that the range of data from standard viscosity measurements is too small to determine the nature of the glass transition.

In this work, we develop an approach for extending the accessible range of viscosities using nonequilibrium simulations. The approach assumes an analytic form for the shear-rate–dependent viscosity that is validated by comparing to the unusually large set of nonequilibrium and equilibrium flow measurements for squalane (19, 20, 22–27). Newtonian viscosities are obtained from two-parameter fits of this analytic form to the high-rate response. Our results agree with experimental values of η_N over 10 orders of magnitude and predict values more than 10 orders of magnitude larger. They also allow a wide range of pressures and densities to be explored. Based on these results, squalane becomes a strong glass-former with a constant energy barrier at high pressures and low temperatures. There is no indication of a finite-temperature divergence in ΔH or viscosity.

Results

Nonequilibrium Shear Stress and Viscosity. Squalane (Fig. 1) is a short hydrocarbon with side branches. The branches inhibit

Significance

As a liquid cools, molecules move more slowly and the viscosity rises. A fundamental question is whether this trend continues smoothly down to zero temperature, or if flow stops at a finite temperature where the material undergoes a transition to a glass phase. Direct measurements of growing viscosities become difficult as the time for motion exceeds years or centuries. We describe and test an approach for obtaining large viscosities using nonequilibrium molecular dynamics simulations. Results agree with existing experiments on the model glass-former squalane and allow viscosities over 10 orders of magnitude larger to be predicted. The temperature dependence at fixed pressure or density is consistent with a gradual slowing of dynamics, rather than a finite-temperature divergence in viscosity.

Author contributions: V.J. and M.O.R. designed research; V.J. and M.O.R. performed research; V.J. performed simulations; V.J. and M.O.R. analyzed data; and V.J. and M.O.R. wrote the paper.

The authors declare no conflict of interest.

This article is a PNAS Direct Submission.

[1]To whom correspondence should be addressed. Email: mr@jhu.edu.

This article contains supporting information online at www.pnas.org/lookup/suppl/doi:10.1073/pnas.1705978114/-/DCSupplemental.

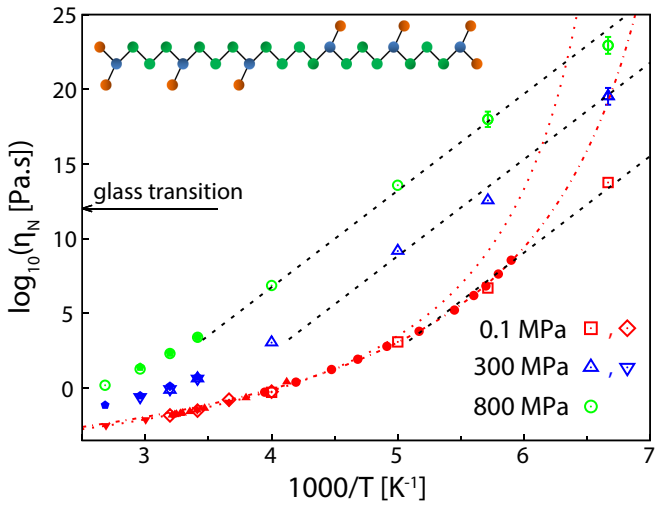

Fig. 1. Newtonian viscosity of squalane as a function of temperature T. η_N is plotted against $1000/T$ for constant pressures of $P = 0.1$ MPa (red), 300 MPa (blue), and 800 MPa (green). Open symbols are our results with η_N evaluated directly from low-rate simulation data (diamonds and upside-down triangles) or obtained from Eyring fits (squares, right-side-up triangles, and circles). Filled symbols are experimental data from ref. 20 (pentagons), ref. 22 (inverted triangles), ref. 23 (triangles), and ref. 19 (circles). Error bars are shown for simulation data when they are larger than the symbol size. Dashed black lines are Arrhenius fits to data at $\eta_N > 10^3$ Pa·s with constant $\Delta H = 1.28$ eV. Red lines are VFT fits to experimental data for $T \geq 240$ K (dotted line) (23) and $T \geq 170$ K (dash-dotted line) (19) that give $T_{g0} = 139$ K and 126 K, respectively. By convention, the glass transition temperature T_g is where the viscosity is 10^{12} Pa·s. (*Inset*) Sketch of squalane showing carbon atoms (circles) and covalent carbon–carbon bonds (lines). Red, green, and blue circles indicate carbon atoms with three, two, and one hydrogen atoms, respectively.

crystallization, making squalane ideal for fundamental studies of the glass transition (19, 22, 23). It has also been widely used as a model fluid in studies of elastohydrodynamic lubrication (20, 24, 26), where lubricants are subjected to extreme pressures P and strain rates $\dot{\gamma}$. In this latter context, the nonequilibrium response of squalane has been measured as a function of $\dot{\gamma}$ for P up to ~ 1 GPa and over a wide range of T (20, 24, 25). We have used standard simulation methods (*Materials and Methods*) to determine the strain-rate–dependent shear stress σ and viscosity at corresponding state points. Although long times are required to reach equilibrium in glassy systems, sheared systems reach steady state in a time of order $1/\dot{\gamma}$, making it possible to obtain the nonequilibrium $\sigma(\dot{\gamma})$ at arbitrary density and temperature for rates as low as 10^5 s^{-1}.

Fig. 2*A* compares experimental and simulation results for the strain rate dependence of σ at room temperature and varying pressure P. Fig. 2*B* shows the nonequilibrium viscosity, $\eta \equiv \sigma/\dot{\gamma}$, calculated from the same data. Experimental data extend up to $\dot{\gamma} \sim 10^4$ s^{-1}, and we have calculated the viscosity down to $\dot{\gamma} \sim 10^5$ s^{-1}. For $P \leq 500$ MPa ($\eta_N < 10^2$ Pa·s), simulation rates are low enough to reach the constant low-rate Newtonian viscosity η_N. For larger pressures and viscosities, we determined η_N by fitting $\eta(\dot{\gamma})$ to the Eyring model (dashed lines in Fig. 2).

The Eyring model (28) is a simple extension of the activation model for viscosity (Eq. **1**) that includes the effect of shear stress. The idea is that the barrier for forward hops (in the direction of shear) decreases linearly with the applied shear stress, whereas the barrier for backward hops (in the reverse direction) rises. The net flow rate $\dot{\gamma}$ can then be calculated from the difference between forward and backward hops (*SI Text*):

$$\dot{\gamma} = \frac{\sigma_E}{\eta_N} \sinh(\sigma/\sigma_E), \qquad [3]$$

where η_N is given by Eq. **1** with the equilibrium barrier $\Delta H(\sigma = 0)$ for a given T and P, and the Eyring stress σ_E characterizes the rate of change of ΔH with σ: $|\partial \Delta H/\partial \sigma| \equiv k_B T/\sigma_E$. One recovers the Newtonian response at $\sigma \ll \sigma_E$. At large stresses, σ rises linearly with $\log \dot{\gamma}$. This linear behavior is clearly evident for high-viscosity systems ($\eta_N > 1$ Pa·s) in Fig. 2*A* and Figs. S1 and S2 and has been observed in elastohydrodynamic lubrication at high rates and pressures (26). A simple straight-line fit at large $\dot{\gamma}$ yields both the Eyring stress and Newtonian viscosity.

Fig. 2 shows that Eyring fits to simulations at $T = 293$ K and $P \geq 300$ MPa provide an excellent description of the numerical data and extrapolate smoothly to the experimental values of the Newtonian viscosity. Fits at other state points are shown in *SI Text*. At very high rates, $\dot{\gamma} > 5 \cdot 10^9$ s^{-1}, the stress rises above the Eyring fit. In this regime, the strain rate is approaching phonon frequencies, leading to new dissipation mechanisms. Experimental results drop slightly below the Eyring fits at the highest rates. This difference may reflect heating under these extreme rates and shear stresses (26) or expansion under shear, because experiments fix the component of the stress tensor in the vorticity direction and allow dilation (29). Both changes would reduce the viscosity compared with our simulations at fixed temperature and volume (*Materials and Methods*).

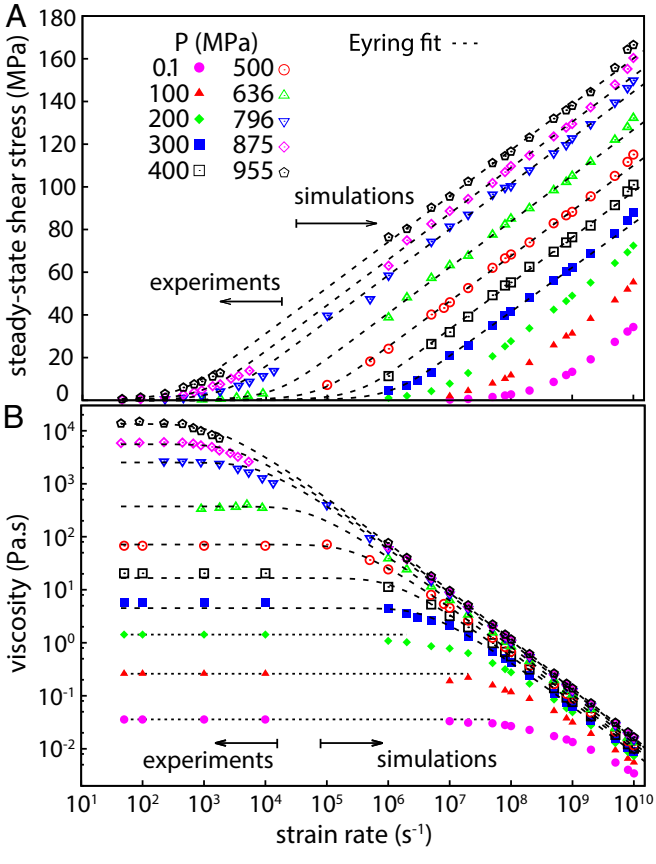

Fig. 2. Steady-state shear stress σ and viscosity η of squalane as a function of strain rate $\dot{\gamma}$. Stress σ vs. $\dot{\gamma}$ at $T = 293$ K for P from 0.1 – 955 MPa (*A*) and viscosity $\sigma/\dot{\gamma}$ vs. $\dot{\gamma}$ (*B*) for the same systems. Symbols for $\dot{\gamma} \geq 10^5$ s^{-1} correspond to MD simulation results, whereas symbols at lower rates are from experiment (20, 24, 25). Black dashed lines are Eyring model fits to simulation data that show the expected linear dependence of stress on $\log \dot{\gamma}$ for high $\dot{\gamma}$. For $P \geq 300$ MPa, the Eyring fit extrapolates to the measured Newtonian viscosity at low rates. For $P \leq 500$ MPa, simulations reach the Newtonian limit (dotted lines) without extrapolation.

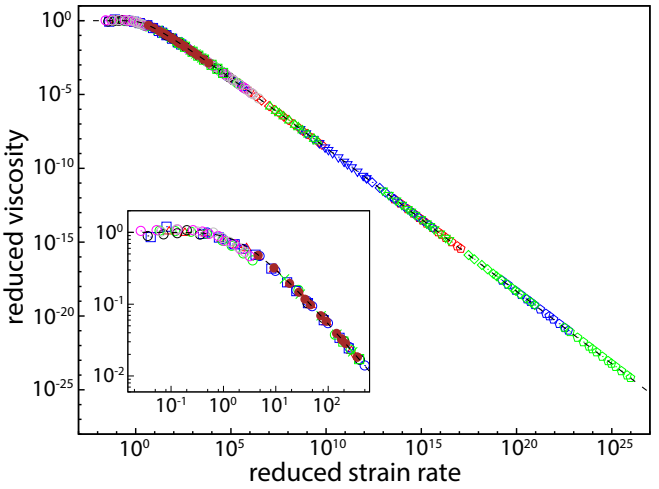

Fig. 3. Collapse of viscosity data from different T and P. Reduced viscosity η/η_N as a function of reduced strain rate $\eta_N\dot{\gamma}/\sigma_E$ for systems with $\eta_N > 1$ Pa·s and $\dot{\gamma} \leq 3 \cdot 10^9 s^{-1}$. Data are for $P = 0.1$ MPa (red), 300 MPa (blue), 636 MPa (black), 800 MPa (green), 875 MPa (magenta), and 955 MPa (gray) at $T =$ 150 K (pentagons), 175 K (diamonds), 200 K (inverted triangles), 250 K (triangles), 293 K (circles), 313 K (squares), and 338 K (crosses). Data for $\rho =$ 0.95 g · cm^{-3} (filled brown circles) at $T = 293$, 313, and 338 K are also shown. Data from both simulations and experiments are used, and the dashed line shows the prediction of the Eyring model. *Inset* expands the low rate region.

Fig. 3 further illustrates the success of Eyring theory in describing all systems with $\eta_N \gtrsim 1$ Pa·s. Viscosity data from different temperatures are frequently collapsed by using the hypothesis of time–temperature superposition (30) (i.e., that as temperature changes, the relaxation time for all modes scales with a single characteristic relaxation time τ_R). When this hypothesis holds, plots of η/η_N against $\dot{\gamma}\tau_R$ collapse onto a universal curve, and data for each T and P reveal part of the curve. A collapse for squalane at a wide range of pressures and temperatures is shown in Fig. 3, with $\tau_R = \eta_N/\sigma_E$. Over almost 30 decades, simulation and experimental data from the glassy regime lie on the analytic solution of the Eyring model.

Variation of Newtonian Viscosity with *T* and *P*. Assuming an Eyring form for the stress vs. strain-rate curves allows us to extract a prediction for η_N from simulations at high rates as long as there is a substantial linear region in plots of σ vs. $\log\dot{\gamma}$. We find that this condition is met whenever $\eta_N \gtrsim 1$ Pa·s. Farther from the glassy regime, the response deviates from the simple Eyring form, indicating that the motion cannot be described by a single activation barrier or rearrangement mechanism. The response is better described by models with a wide range of characteristic times, such as the modified power law in the Carreau formula that is often used to model simple fluids (31). Fortunately, the rapid dynamics in this regime means that we do not need to assume any form for the viscosity. Instead, values of η_N can be determined directly from simulations up to $\eta_N \sim 10^2$ Pa·s.

We have explored the effect of temperature and pressure on viscosity over a large range of parameters by combining direct evaluations of η_N with Eyring fits. Some of the data are summarized in Fig. 1. They agree with available experimental data from 10^{-3} to 10^8 Pa·s and predict η_N up to 10^{22} Pa·s.

All of the simulation results in Fig. 1 show a cross-over from fragile, super-Arrhenius behavior to strong, Arrhenius behavior as T decreases. At each pressure, the cross-over occurs when the viscosity exceeds $\sim 10^3$ Pa·s. The corresponding cross-over temperature T_a increases with increasing pressure. Dashed fit lines in Fig. 1 show that data for $T \leq T_a$ and $\eta_N \gtrsim 10^3$ Pa·s can be described by a pressure- and temperature-independent activation barrier. Expressing the pressure-dependent η_0 in terms of T_a, we find:

$$\eta_N = \eta_a \exp[(\Delta H/k_B)\,(1/T - 1/T_a)], \quad T \leq T_a, \qquad [4]$$

with $\eta_a = 10^3$ Pa·s, $\Delta H = 1.28$ eV, and $T_a \sim 197$, 245, 292 K for $P = 0.1$, 300, 800 MPa, respectively.

Past VFT fits to experimental data in Fig. 1 are clearly inconsistent with our extension of ambient pressure results to lower temperatures. Additional bounds on the rise in η_N are implied by our high-pressure results. For a simple molecule like squalane, viscosity rises monotonically with pressure at fixed temperature (20). Any super-Arrhenius fit to low-pressure data with $T_{g0} \gtrsim 100$ K rises rapidly above the Arrhenius behavior seen in our high-pressure results, whereas fits with $T_{g0} \lesssim 110$ K can only fit a portion of the experimental data. Thus, our extrapolated results are inconsistent with a finite temperature divergence of η_N for squalane.

Separating the Roles of *T* and Density. As noted in experimental and simulation studies of other fluids, measurements of η_N at constant pressure mix the effects of temperature and density ρ because of thermal expansion (32–34). Fig. 4 shows η_N as a function of ρ for different P and T. For low viscosities, the change in viscosity produced by a 10% increase in ρ is comparable with that from a similar change in T (338 to 293 K). As the viscosity increases, variations with temperature become more dramatic than changes with density. Refs. 32 and 33 showed similar behavior in experimental data for other glass-formers and concluded that temperature dominates changes in η_N at large viscosities.

Simulations allow us to easily determine the variation of η_N with T at constant density instead of constant pressure. Fig. 5 contrasts the ambient pressure data from Fig. 1 with the rise in η_N for two constant densities, 0.95 and 1.0 g/cm^3. The corresponding temperatures at ambient pressure in an equilibrium fluid can be estimated by extrapolating the linear thermal expansion at $T \geq 250$ K. We find 96 and 22 K, respectively. These values overestimate the temperature because the thermal

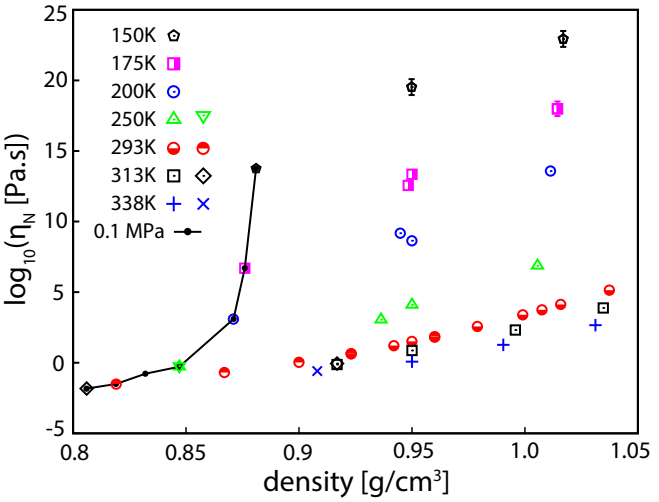

Fig. 4. Newtonian viscosity of squalane as a function of density. Symbols indicate changes at constant $T = 150$, 175, 200, 250, 293, 313, and 338 K and at constant $P = 0.1$ MPa. Crosses, diamonds, light-side-down Janus circles, and upside-down triangles indicate results with η_N evaluated directly using low-rate simulation data. Pluses, squares, light-side-up Janus circles, and right-side-up triangles denote estimates of η_N obtained from Eyring fits. Note that the increase in η_N with fractional changes in T is larger than with fractional changes in ρ, and the difference grows at large η_N. Similar results have been obtained in experiments on other glasses (32, 33).

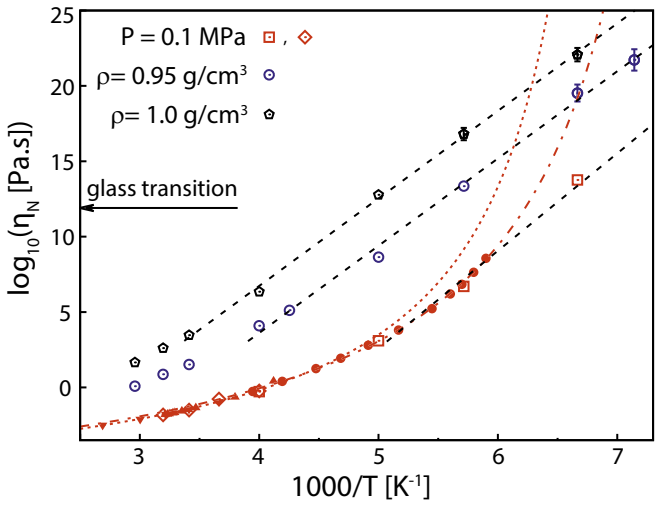

Fig. 5. Newtonian viscosity of squalane as a function of T for fixed density. Results for 0.95 g/cm^3 (blue circles) and 1.0 g/cm^3 (black pentagons) are compared with ambient pressure results from Fig. 1 (red). Error bars are shown for simulation data when they are larger than the symbol size. Black dashed lines are Arrhenius fits, and red lines show VFT fits with $T_{g0} = 139$ K (dashed) and 126 K (dash-dotted) (19, 23). By convention, the glass transition temperature T_g is where $\eta_N = 10^{12}$ Pa·s.

expansion coefficient decreases with decreasing temperature and goes to zero at low T due to quantum effects.

Viscosities for both constant densities exhibit a clear transition to Arrhenius behavior. As for constant pressure plots, the transition occurs for $\eta_N \gtrsim 10^3$ Pa·s. The activation barrier, corresponding to the slope of dashed line fits in Fig. 5, is insensitive to density, but slightly smaller than the value for ambient pressure results. This difference is expected because the density rises with decreasing T in the constant pressure ensemble. The fact that the difference in activation barriers for constant P and ρ results is small provides further evidence that density plays a weaker role than temperature in the rise of η_N (32, 33).

The Arrhenius behavior for constant density in Fig. 5 provides further constraints on fits to any model like VFT that predicts a diverging viscosity at finite T. It also eliminates a potential uncertainty in the constant pressure results of Fig. 1. The quench rates in our simulations are much higher than experiment, and the density at a given P and T is known to depend on both quench rate and subsequent aging. This rate dependence might lead to different densities in our simulations and experiments at ambient pressure. Fig. 4 shows that the sensitivity to density is low. The constant density data in Fig. 5 are at much higher densities than expected at ambient pressure down to previous estimates of T_{g0} (≥ 126 K) and provide strong bounds for fits to VFT models.

Discussion and Conclusions

The results presented above show that Newtonian viscosities can be obtained over a very wide range of temperatures and densities by using nonequilibrium molecular dynamics (MD) simulations. For η_N up to 10^2 Pa·s, simulation rates are slow enough to reach the Newtonian regime, and η_N is obtained directly. For $\eta_N > 1$ Pa·s, the viscosity is obtained by extrapolating Eyring fits to high-rate data. The remarkably large set of equilibrium and nonequilibrium experiments on the typical fragile glass-former squalane allow a detailed test of the extrapolation. We find that Eyring fits to high-rate simulations extrapolate smoothly through experimental data that reach nearly the same high strain rates. In addition, the method produces values of η_N that agree with experimental measurements for a wide range of pressures and temperatures and for η_N between 10^{-3} and 10^8 Pa·s. Although there is no guarantee that the Eyring extrapolation will be valid outside the range we have tested it, it provides a straightforward method for exploring a wide parameter space and very large viscosities. The approach is readily extendable to other small-molecule glass-formers. For polymers and other large molecules, the shear thinning associated with molecular alignment may cover many decades in plots like Fig. 3, making Eyring fits difficult.

Based on the agreement with existing experiments, we have determined the scaling of squalane's viscosity for T between 140 and 338 K, pressures up to 1 GPa, and densities between 0.8 and 1.05 g/cm^3. Our extrapolated data show no evidence of diverging viscosity at finite T_{g0}. For both constant pressure and constant density, we see a transition to Arrhenius behavior for $\eta_N \gtrsim 10^3$ Pa·s.

Hecksher et al. had noted that it was difficult to rule out a diverging viscosity at a finite T_{g0} based on existing experimental data (21). Our data extend over 25 decades in viscosity, whereas the experiments they considered spanned less than 10 decades. Moreover, our high-pressure and -density data put tight bounds on any rapid rise in η_N at ambient pressure. In particular, they are inconsistent with past fits to the VFT relation.

The conclusion that there is a cross-over from super-Arrhenius behavior at low η_N to Arrhenius at high η_N is consistent with recent aging studies of 20-million-year-old amber (9) and some previous studies of viscosity and transport (35–37). In particular, Mallamace et al. analyzed existing viscosity data for 48 different glass-forming liquids at ambient pressure and found a cross-over to Arrhenius behavior at the lowest temperatures when the viscosity exceeded $\sim 10^2$ Pa-s (36). Our results for squalane agree with this finding, although our data suggest a slightly larger cross-over viscosity of $\sim 10^3$ Pa·s. Moreover, Figs. 1 and 5 show that the same cross-over occurs at higher pressure and different constant densities.

Our results indicate that there are substantial changes in structure in the super-Arrhenius regime at low η_N. For $\eta_N < 1$ Pa·s, the nonequilibrium response is not well fit by Eyring theory. In this regime, squalane is a simple fluid that is not described by activated dynamics over a single barrier. The rheology is consistent with common models that assume a broad spectrum of relaxation times (31). For $\eta_N > 1$ Pa·s, the nonequilibrium viscosity is consistent with the Eyring model and a single activation barrier ΔH. The Eyring fit spans a wider range of shear rates as η_N rises. The slow variation in ΔH as η_N rises to 10^3 Pa·s indicates an ongoing evolution in structure that saturates for $\eta_N > 10^3$ Pa·s.

A number of interesting studies have found signatures of a true finite-temperature phase transition, including changes in high-order correlation functions that indicate a growing correlation length (14, 15). It has been difficult for these approaches to access low enough temperatures to see increases in length scale by more than an order of magnitude. One possibility is that correlations saturate as T decreases (12), just as ΔH saturates in our simulations. In many cases, these studies correspond to $\eta_N < 10^3$ Pa·s (viscosities $< 10^6$ times the high temperature value), where we also see evidence of changing structure. It is also possible that there is a true phase transition, but that it does not correspond to a diverging viscosity (38). For example, even defected crystals can flow through Eyring-like activation processes at high stresses. Finally, our nonequilibrium simulations may destroy long-range and -time correlations that would show up as deviations from Eyring fits at correspondingly low rates. Missing such correlations could limit the increase in η_N obtained with our approach. However, increases in correlation length have been observed at much lower viscosities than 10^8 Pa·s, and our approach describes experiments up to the highest η_N reported.

Our results provide testable predictions for the high-pressure and low-temperature viscosity of squalane. Direct measurements

of the highest viscosities in Fig. 1 are impractical because the relaxation times, η_N/σ_E, become comparable to the age of the universe. However, nonequilibrium measurements can be made at experimentally accessible rates to validate our extrapolation from much higher rates. Combining experiment and simulation as in Fig. 2 may greatly reduce the uncertainty in η_N and allow tighter limits on viscosity models used in studies of a wide range of small-molecule glass-formers.

Materials and Methods

Squalane, or 2,6,10,15,19,23-hexamethyltetracosane ($C_{30}H_{62}$), is a branched alkane with a C_{24} backbone and six methyl side groups placed symmetrically about the backbone center. Past studies of squalane and similar alkanes showed that united atom (UA) potentials accurately describe the viscosity at ambient pressure (39–42). As shown in the schematic in Fig. 1, each UA represents a carbon and its covalently bonded hydrogens. UAs representing CH_3, CH_2 and CH groups interact with different potentials.

We use the potential parameters that Mondello and Grest used for squalane (40). Within each molecule, UAs interact with a harmonic bond-stretching term, a harmonic bond-bending term, a torsional potential characterizing the rotational barrier around nonterminal bonds, and a harmonic bending term to prevent umbrella (sp_3) inversion at tertiary carbon branch points. Atoms on different molecules or separated by four or more bonds on the same molecule interact with a 6–12 Lennard–Jones potential. The model gives accurate values of the viscosity at ambient pressure, although the density is systematically too high. We checked that treating hydrogens separately by using an all-atom potential developed for high pressure (43) gave consistent results for the viscosity at a given pressure and more accurate densities.

To generate equilibrium squalane states, we prepared a melt configuration composed of $N_m = 125$ molecules ($N = 3750$ UAs) in a periodic unit cell with cubic geometry at room temperature $T = 293$ K and ambient pressure $P = 0.1$ MPa. After equilibrating this low-viscosity state, the volume was decreased over 1 ns to the estimated density for the desired pressure. The system was then equilibrated alternately at constant pressure and density over an additional 4 ns to obtain the correct density at the chosen P. The equilibration times were increased by up to a factor of 10 as P increased. States at different temperatures were created from the room-temperature state by first changing T at <15 K/ns at constant volume. The appropriate density was then found by using alternating constant pressure and density runs over 40 ns. Different seeds and protocols gave equivalent results on the scale of the symbol size in our plots. We also found the same results for systems with eight times as many molecules (*SI Text* and Fig. S3).

The steady-state shear stress was obtained with standard nonequilibrium MD methods (44) in LAMMPS (45). Sample input scripts and potential parameters are available in Datasets S1–S3. The periodic box was deformed to impose simple shear (planar Couette flow) at fixed density and strain rate $\dot{\gamma} = \delta u_x/\delta y$ by using the SLLOD equations of motion (44). Here, u_x is the streaming velocity in the flow (x) direction, and the velocity gradient is along the y axis. Constant temperature was maintained with a Nose–Hoover thermostat, and we checked that it maintained constant T and did not affect the shear stress until strain rates higher than those reported here ($> 10^{10}$ s^{-1}). The stress and internal structure were monitored to determine when the system reached steady state. Strains of up to 100 were required. The shear stress σ was then averaged to reduce the statistical errors, which are indicated when they are larger than symbols in the figures.

As noted in *Results*, our Eyring fits agree with experimental measurements of the Newtonian viscosity, but differ slightly from measurements at the highest rates for $P = 796$, 875, and 955 MPa (Fig. 2). We attribute this finding to small differences between the ensembles. There may be some heating and shear dilation in the experiments. Both effects would produce the observed decrease in experimental viscosities. A quantitative estimate of the shift is difficult because of uncertainties in the thermal and mechanical coupling between the sample and viscometer, and the shift disappears in the Newtonian limit.

To isolate the effect of temperature on the rise of viscosity and obtain stricter bounds on squalane viscosity at ambient pressure, we performed simulations at constant density. We extrapolated the high T results at ambient pressure to obtain upper bounds for the density ρ at a given temperature. For $T = 96$ K and 22 K, we find bounds of 0.95 and 1.0 g cm^{-3}, respectively. Fig. S2 shows the steady-state shear stress at $\rho = 0.95$ g cm^{-3}. Eyring fits that are used to extract the Newtonian viscosity are also shown. Simulations of shear at a given density reach steady state in a time of order $1/\dot{\gamma}$, ensuring that we obtain converged results for σ at the chosen density and rate.

ACKNOWLEDGMENTS. We thank Scott Bair, Robert Leheny, Gregory McKenna, and Hugh Spikes for useful discussions; and the Maryland Advanced Research Computing Center and Big Red II Supercomputer at Indiana University for computing resources. This work was supported by the Army Research Laboratory under the Materials in Extreme Dynamic Environments Collaborative Research Alliance through Grant W911NF-12-2-0022 and the Theoretical Interdisciplinary Physics and Astrophysics Center at Johns Hopkins University.

1. Angell CA (1995) Formation of glasses from liquids and biopolymers. *Science* 267:1924–1935.
2. Ediger MD, Angell CA, Nagel SR (1996) Supercooled liquids and glasses. *J Phys Chem* 100:13200–13212.
3. Berthier L, et al. (2005) Direct experimental evidence of a growing length scale accompanying the glass transition. *Science* 310:1797–1800.
4. Lubchenko V, Wolynes PG (2007) Theory of structural glasses and supercooled liquids. *Annu Rev Phys Chem* 58:235–266.
5. Dyre JC (2006) Colloquium: The glass transition and elastic models of glassforming liquids. *Rev Mod Phys* 78:953–972.
6. Debenedetti PG, Stillinger FH (2001) Supercooled liquids and the glass transition. *Nature* 410:259–267.
7. Kivelson SA, Tarjus G (2008) In search of a theory of supercooled liquids. *Nat Mater* 7:831–833.
8. Chandler D, Garrahan JP (2010) Dynamics on the way to forming glass: Bubbles in space-time. *Annu Rev Phys Chem* 61:191–217.
9. Zhao J, Simon SL, McKenna GB (2013) Using 20-million-year-old amber to test the super-Arrhenius behaviour of glass forming systems. *Nat Commun* 4:1783.
10. Berthier L, Coslovich D (2014) Novel approach to numerical measurements of the configurational entropy in supercooled liquids. *Proc Natl Acad Sci USA* 111:11668–11672.
11. Casalini R, Roland CM (2005) Scaling of the supercooled dynamics and its relation to the pressure dependences of the dynamic crossover and the fragility of glass formers. *Phys Rev B* 71:014210.
12. Angelini MC, Biroli G (2017) Real space renormalization group theory of disordered models of glasses. *Proc Natl Acad Sci USA* 114:3328–3333.
13. Adam G, Gibbs JH (1965) On the temperature dependence of cooperative relaxation properties in glassforming liquids. *J Chem Phys* 43:139–146.
14. Albert S, et al. (2016) Fifth-order susceptibility unveils growth of thermodynamic amorphous order in glassformers. *Science* 352:1308–1311.
15. Kob W, Donati C, Plimpton SJ, Poole PH, Glotzer SC (1997) Dynamical heterogeneities in a supercooled Lennard-Jones liquid. *Phys Rev Lett* 79:2827–2830.
16. Vogel H (1921) Das temperaturabh angigkeitsgesetz der viskosit at von fl ussigkeiten. *Phys Zeit* 22:645–646.
17. Fulcher GS (1925) Analysis of recent measurements of the viscosity of glasses. *J Am Ceram Soc* 8:339–355.
18. Tammann G (1925) Glasses as supercooled liquids. *J Soc Glass Technol* 9:166–185.
19. Deegan RD, Leheny RL, Menon N, Nagel SR, Venerus DC (1999) Dynamic shear modulus of tricresyl phosphate and squalane. *J Phys Chem B* 103:4066–4070.
20. Bair S (2006) Reference liquids for quantitative elastohydrodynamics: Selection and rheological characterization. *Tribol Lett* 22:197–206.
21. Hecksher T, Nielsen AI, Olsen NB, Dyre JC (2008) Little evidence for dynamic divergences in ultraviscous molecular liquids. *Nat Phys* 4:737–741.
22. Dixon JA, Webb W, Steele WA (1962) *Properties of Hydrocarbons of High-Molecular Weight Synthesized by Research Project 42 of The American Petroleum Institute, Pennsylvania State University* (American Petroleum Institute, Washington, DC).
23. Barlow AJ, Erginsav A (1972) Viscoelastic retardation of supercooled liquids. *Proc Math Phys Eng Sci* 327:175–190.
24. Bair S (2002) The high pressure rheology of some simple model hydrocarbons. *Proc IME J J Eng Tribol* 216:139–149.
25. Bair S, McCabe C, Cummings PT (2002) Comparison of nonequilibrium molecular dynamics with experimental measurements in the nonlinear shear-thinning regime. *Phys Rev Lett* 88:058302.
26. Spikes H, Jie Z (2014) History, origins and prediction of elastohydrodynamic friction. *Tribol Lett* 56:1–25.
27. Schmidt KAG, et al. (2015) New experimental data and reference models for the viscosity and density of squalane. *J Chem Eng Data* 60:137–150.
28. Eyring H (1936) Viscosity, plasticity, and diffusion as examples of absolute reaction rates. *J Chem Phys* 4:283–291.
29. Bair S, Winer WO (1993) A new high-pressure, high-shear stress viscometer and results for lubricants. *Tribol Trans* 36:721–725.
30. Ferry JD (1980) *Viscoelastic Properties of Polymers* (Wiley, New York).
31. Heyes DM (1986) Non-Newtonian behaviour of simple liquids. *J Newt Fluid Mech* 21:137–155.
32. Ferrer ML, et al. (1998) Supercooled liquids and the glass transition: Temperature as the control variable. *J Chem Phys* 109:8010–8015.
33. Tarjus G, Kivelson D, Mossa S, Alba-Simionesco C (2004) Disentangling density and temperature effects in the viscous slowing down of glassforming liquids. *J Chem Phys* 120:6135–6141.

34. Alba-Simionesco C, Kivelson D, Tarjus G (2002) Temperature, density, and pressure dependence of relaxation times in supercooled liquids. *J Chem Phys* 116:5033–5038.
35. Elmatad YS, Chandler D, Garrahan JP (2009) Corresponding states of structural glass formers. *J Phys Chem B* 113:5563–5567.
36. Mallamace F, et al. (2010) Transport properties of glassforming liquids suggest that dynamic crossover temperature is as important as the glass transition temperature. *Proc Natl Acad Sci USA* 107:22457–22462.
37. Xu Y, Petrik NG, Smith RS, Kay BD, Kimmel GA (2016) Growth rate of crystalline ice and the diffusivity of supercooled water from 126 to 262 K. *Proc Natl Acad Sci USA* 113:14921–14925.
38. DiMarzio EA, Yang AJM (1997) Configurational entropy approach to the kinetics of glasses. *J Res Natl Inst Stand Tech* 102:135–157.
39. Seipmann IJ, Karaborni S, Smit B (1993) Simulating the critical behaviour of complex fluids. *Nature* 365:330–332.
40. Mondello M, Grest GS (1995) Molecular dynamics of linear and branched alkanes. *J Chem Phys* 103:7156–7165.
41. Mondello M, Grest GS, Garcia AR, Silbernagel BG (1996) Molecular dynamics of linear and branched alkanes: Simulations and nuclear magnetic resonance results. *J Chem Phys* 105:5208–5215.
42. Moore JD, Cui ST, Cochran HD, Cummings PT (2000) Rheology of lubricant basestocks: A molecular dynamics study of C30 isomers. *J Chem Phys* 113:8833–8840.
43. O'Connor TC, Andzelm J, Robbins MO (2015) AIREBO-M: A reactive model for hydrocarbons at extreme pressures. *J Chem Phys* 142:024903.
44. Evans DJ, Morris GP (1990) *Statistical Mechanics of Nonequilibrium Liquids* (Academic, New York).
45. Plimpton SJ (1995) Fast parallel algorithms for short-range molecular dynamics. *J Comput Phys* 107:1–19.